Optimizing the ionization and energy absorption of laser-irradiated clusters

M. Kundu and D. Bauer
Max-Planck-Institut für Kernphysik, Postfach 103980, 69029 Heidelberg, Germany
(Dated: February 2, 2008)

It is known that rare-gas or metal clusters absorb incident laser energy very efficiently. However, due to the intricate dependencies on all the laser and cluster parameters it is difficult to predict under which circumstances ionization and energy absorption is optimal. With the help of three-dimensional particle-in-cell simulations of xenon clusters (up to 17256 atoms) we find that for a given laser pulse energy and cluster an optimum wavelength exists which corresponds to the approximate wavelength of the transient, linear Mie-resonance of the ionizing cluster at an early stage of negligible expansion. In a single ultrashort laser pulse, the linear resonance at this optimum wavelength yields much higher absorption efficiency than in the conventional, dual-pulse pump-probe set-up of linear resonance during cluster expansion.

PACS numbers: 36.40.Gk, 52.25.Os, 52.50.Jm

I. INTRODUCTION

The interaction of rare-gas and metal clusters with intense laser light has drawn close attention during the last ten years. Reasons for this large interest are (among others) the high charge states [1, 2, 3, 4, 5, 6, 7, 8, 9] and the high energies of both ions [1, 2, 3, 4, 6, 7, 8, 9, 10, 11, 12] and electrons [10, 12, 13, 14, 15] observed (see [16] for a recent review).

The laser-cluster interaction scenario may be qualitatively summarized as follows. Electrons leave their "parent" atoms ("inner ionization") and absorb further laser energy while moving in the cluster potential formed by the ionic background. Some electrons may leave the cluster ("outer ionization"), leaving behind a net positively charged nanoplasma. The total electric field consists of the laser plus the space charge field. It may exceed the pure laser field in certain spatial regions and thus may liberate further electrons from their parent ions (which would remain bound if there was the laser field alone). This enhanced inner ionization is called "ionization ignition" [17, 18, 19, 20, 21, 22]. Ionization ignition locally continues until the total field drops below the threshold field required to liberate further electrons. The ionic background expands because of Coulomb repulsion and hydrodynamic pressure, which ultimately leads to the energetic ions observed in experiments. Because of the complex interplay between inner ionization, outer ionization, and ionic expansion it is far from trivial to predict quantitatively mean or highest charge states, the absorbed laser energy, or other observables and their dependence on the laser parameters and the cluster decomposition.

One of the goals in laser-cluster experiments and simulations is to convert as much laser energy as possible into energetic particles. This can be achieved by optimizing the outer ionization degree, i.e., by removing as many electrons as possible from the cluster in order to generate high charge states so that the asymptotic ion energy (and thus the total absorbed energy) after Coulomb explosion is largest.

One way to increase the charge states and the ion energy is to dope a cluster with atomic/molecular species of low ionization potential [23, 24]. An almost two-fold increase of the highest charge states were obtained experimentally with argon clusters doped with water molecules [25].

Experimental results for xenon and silver clusters embedded in helium droplets were reported in Ref. [26]. The pulse duration and the sign of the chirp of a laser-pulse also affect ion charge states and ion energies [27]. Enhanced inner ionization of rare-gas and metal clusters irradiated by a sequence of dual laser pulses were observed [11, 26, 28, 29] experimentally. In these kinds of experiments one should adjust the delay time between pump and probe pulse such that the cluster expands sufficiently to meet the linear resonance $\omega_{\rm Mie} = \omega_{\rm l}$ with the probe pulse, where $\omega_{\rm Mie}$ is the Mie-plasmon frequency and $\omega_{\rm l}$ is the laser frequency. Vlasov simulations [26] and semi-classical simulations [30] of a small Xe_{40} cluster subject to such a pump-probe setup showed an enhancement of the ion charge states. An optimum control multi-pulse simulation has also been performed [31].

In this work we investigate the effect of the laser wavelength by three-dimensional particle-in-cell (PIC) simulations. The goal is to find an optimum wavelength for a fixed laser intensity and a given cluster. At this optimum wavelength (which turns out to be in the ultraviolet (UV) regime for the Xe clusters under consideration) a single ultrashort laser pulse is shown to be much more efficient than the "conventional" dual-pulse pump-probe setup.

Experimental signatures of enhanced x-ray yields and high charge states at short wavelengths [32, 33, 34] indicate a clear impact of the laser wavelength on the laser-cluster interaction. Free electron laser (FEL) cluster experiments [35] at the DESY facility, Hamburg, and a recent x-ray laser-cluster experiment [36] down to wavelengths < 100 nm also showed enhanced ionization.

Contrary to our findings recent molecular dynamics simulations [37] concluded that (i) there is no influence of the laser wavelength on the charging of clusters in the regime $100 - 800$ nm for a laser intensity $\approx 10^{16}\mathrm{Wcm}^{-2}$ and (ii) that linear resonance plays no role, thus threat-

ening the basis of the nanoplasma model [38]. Similar conclusions were reported by the same authors in Refs. [39, 40].

We consider short laser pulses in this work. Most of the earlier works were reported for the long-pulse regime where linear resonance (LR) absorption [26, 30, 31, 38, 41, 42, 43, 44, 45] occurs during the expanding phase of a cluster when the Mie-plasma frequency drops sufficiently so that the laser frequency can be met. At the time of LR the space charge field inside the cluster is strongly enhanced, leading to efficient ionization ignition.

The paper is organized as follows. In Sec. II we briefly describe the simulation method and discuss the ionization of a cluster by a short laser pulse in Sec. III. In Sec. IV pump-probe simulation results are presented while Sec. V is devoted to the laser wavelength dependence of the cluster dynamics. A possibility to achieve 100% outer ionization is also discussed in Sec. V before we summarize the work in Sec. VI. Unless stated otherwise we use atomic units (a.u.).

II. DETAILS OF THE SIMULATION

Details of our PIC code are already described in Refs. [46, 47].

For the inner ionization we apply the so-called Bethe-rule or over-the-barrier ionization (OBI) model [48]. According to OBI an atom or ion is ionized if the total field satisfies

$$|\boldsymbol{E}_{\rm l}(t) + \boldsymbol{E}_{\rm sc}(\boldsymbol{R}_j, t)| \geq I_{\rm p}^2(\mathcal{Z})/4\mathcal{Z} \qquad (1)$$

at individual ion locations $\boldsymbol{R}_j$. Here $\mathcal{Z}$ is the charge state (after ionization), $I_{\rm p}(\mathcal{Z})$ is the respective ionization potential and $\boldsymbol{E}_{\rm sc}(\boldsymbol{R}_j, t)$ is the space charge field. In the absence of $\boldsymbol{E}_{\rm sc}(\boldsymbol{R}_j, t)$ ionization is caused by the laser field, known as optical field ionization (OFI).

In this work we shall vary the wavelength down to 100 nm at an intensity $5 \times 10^{16}\mathrm{Wcm}^{-2}$, which raises the questions (i) whether such lasers are available and (ii) whether the Bethe-rule (1) is applicable. With the development of new generation FEL lasers [49, 50] the answer to (i) is clearly affirmative. As regards the ionization model (ii), at short wavelengths ionization rather proceeds via multiphoton ionization than via tunneling or over-the-barrier ionization so that the Bethe-model (where the ionization probability switches from zero to unity once a certain threshold field is reached) may not yield the precise charging dynamics of the clusters at short wavelengths. However, the final charge state distribution should remain unaffected by the details of the ionization model [40] at least qualitatively.

Only collisionless absorption mechanisms are incorporated in standard PIC simulations. The neglect of particle collisions is an approximation which is the more valid the smaller the clusters, the higher the laser intensities, and the longer the laser wavelengths are (see, e.g., [19, 20, 21, 22, 51, 52]). Since collisions can be expected to increase both energy absorption and ionization, our results from collisionless PIC calculations may be considered close to reality for wavelengths $\gtrapprox 400\,$nm but slightly underestimating the real charge states and the real absorbed energy for shorter wavelengths.

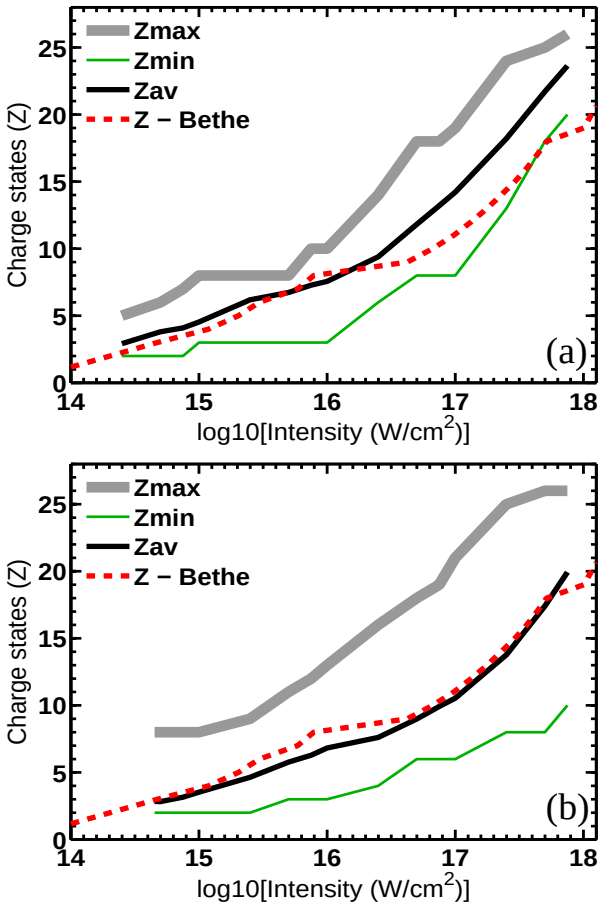

FIG. 1: (Color online) Maximum ion charge $\mathcal{Z}_{\rm max}$ (thick solid), minimum ion charge $\mathcal{Z}_{\rm min}$ (thin solid), average ion charge $\mathcal{Z}_{\rm av}$ (bold black) and the ion charge predicted by OFI alone (dashed) vs peak laser intensity for (a) a Xe_{2176} cluster of radius $R_0 \approx 3.54$ nm and (b) a Xe_{17256} cluster of radius $R_0 \approx 7$ nm in an $n = 8$ cycle laser pulse $E_{\rm l}(t) = E_0 \sin^2(\omega_{\rm l} t/2n)\cos(\omega_{\rm l} t)$ of wavelength $\lambda_{\rm l} = 800$ nm.

III. IONIZATION OF A CLUSTER BY A SINGLE SHORT PULSE

First we study the response of a xenon cluster in a linearly polarized $n = 8$-cycle laser pulse of electric field strength $E_{\rm l}(t) = E_0 \sin^2(\omega_{\rm l} t/2n)\cos(\omega_{\rm l} t)$ and wavelength $\lambda_{\rm l} = 800$ nm. Different ionic charge states are self-consistently produced during the laser pulses according to the Bethe rule (1).

Figure 1a shows the maximum charge state $\mathcal{Z}_{\rm max}$, the minimum charge state $\mathcal{Z}_{\rm min}$, and the average charge state $\mathcal{Z}_{\rm av}$ (defined as the total charge of the cluster divided by

the number of atoms N) and the charge state predicted by the OFI ("Z-Bethe" curve) vs peak laser intensity for a Xe_N cluster ($N = 2176$) of initial radius $R_0 \approx 3.54$ nm after the pulse (i.e., after ≈ 22 fs). The maximum charge state $\mathcal{Z}_{\max}$ varies from $\mathcal{Z} = 5$ to $\mathcal{Z} = 26$ as the laser intensity increases from $2.5\times10^{14}\mathrm{Wcm}^{-2}$ to $7.5\times10^{17}\mathrm{Wcm}^{-2}$. The higher value of $\mathcal{Z}_{\max}$ above the value predicted by the OFI is clearly due to ionization ignition. Those maximum charge states $\mathcal{Z}_{\max}$ are mainly acquired by the ions at the cluster periphery where the space charge field is highest. Inside the cluster the total field falls below the ionization thresholds due to the decreasing space charge produced by the ionic background as well as due to the screening of the laser field by the cluster electrons. The ions close to the cluster center have minimum charge states $\mathcal{Z}_{\min} = 2 - 20$ at laser intensities between $2.5\times10^{14}\mathrm{Wcm}^{-2} - 7.5\times10^{17}\mathrm{Wcm}^{-2}$. The value of $\mathcal{Z}_{\min}$ remains much lower than predicted by the OFI for almost all laser intensities $< 5.0\times10^{17}\mathrm{Wcm}^{-2}$. The average charge $\mathcal{Z}_{\mathrm{av}}$ remains close to (but slightly higher than) the OFI predicted values at intensities $< 7.5\times10^{15}\mathrm{Wcm}^{-2}$. Also $\mathcal{Z}_{\max} = 8$ and $\mathcal{Z}_{\min} = 3$ do not change between the intensities $10^{15}\mathrm{Wcm}^{-2} - 7.5\times10^{15}\mathrm{Wcm}^{-2}$ but $\mathcal{Z}_{\mathrm{av}}$ increases slowly as more ions from the cluster center towards the periphery acquire higher charge states $3 \rightarrow 8$. The value of $\mathcal{Z}_{\max}$ remains constant, $\mathcal{Z} = 8$, due to the removal of all electrons from the $5s^2p^6$ shell of the Xe atoms close to the cluster boundary. As the intensity $\approx 7.5\times10^{15}\mathrm{Wcm}^{-2}$ is approached the laser field is strongly shielded from the central part of the cluster, and outer ionization as well as ionization ignition tend to saturate. As a consequence $\mathcal{Z}_{\mathrm{av}}$ grows slowly between the intensities $\approx 5\times10^{15}\mathrm{Wcm}^{-2} - 10^{16}\mathrm{Wcm}^{-2}$. Unless a threshold intensity $\approx 10^{16}\mathrm{Wcm}^{-2}$ is crossed further electrons from the cluster cannot be removed, which was already seen in previous model and numerical calculations [46, 53, 54, 55]. At higher intensities $> 10^{16}\mathrm{Wcm}^{-2}$ outer ionization and ionization ignition increases again, leading to an increase of $\mathcal{Z}_{\mathrm{av}}$ beyond the values predicted by the OFI due to the strong increase of both $\mathcal{Z}_{\max}$ and $\mathcal{Z}_{\min}$.

It is commonly believed that ionization ignition becomes increasingly pronounced with increasing cluster size. Figure 1b shows $\mathcal{Z}_{\max}$, $\mathcal{Z}_{\min}$, $\mathcal{Z}_{\mathrm{av}}$, and the charge states predicted by the OFI vs the peak laser intensities for a bigger Xe_N cluster ($N = 17256$) of initial radius $R_0 \approx 7$ nm. $\mathcal{Z}_{\max}$ varies between $8 - 26$, exceeding again the charge states predicted by OFI alone. Below the intensity $10^{17}\mathrm{Wcm}^{-2}$ $\mathcal{Z}_{\max}$ is higher by a factor of ≈ 2 compared to the OFI value ("Z-Bethe" curve). Although $\mathcal{Z}_{\max}$ remains much higher, the average ion charge $\mathcal{Z}_{\mathrm{av}}$ (in Fig. 1b) is below the charge states predicted by the OFI for most of the laser intensities. Most of the ions closer to the cluster center acquire charge states $\mathcal{Z}_{\min} = 2 - 10$ which are even lower than for the smaller cluster (Fig. 1a) at the corresponding intensities. Hence, ionization ignition is indeed responsible for the highest charge states $\mathcal{Z}_{\max}$ which increase with the cluster size (as seen in Fig. 1). However, exactly because of the same mechanism a bigger cluster will capture more electrons (whose outer ionization would require much higher laser intensities than in the case of a smaller cluster). The presence of more electrons in the central region will screen the laser field more efficiently. As a result both $\mathcal{Z}_{\mathrm{av}}$ as well as $\mathcal{Z}_{\min}$ (in Fig. 1b) drop below the corresponding values for the smaller cluster (Fig. 1a).

We conclude that an increasing cluster size (and thus increased ionization ignition of, at least, the ions located close to the cluster boundary) does not always lead to a higher average charge state. Our aim is to increase not only the highest charge states but also the average ion charge beyond the OFI predicted value through the charging of more ions in the central part of the cluster. In the following sections we study several approaches to achieve this goal.

IV. IONIZATION BY DELAYED PULSES: A PUMP-PROBE SIMULATION

In this section we illustrate the "pump-probe" method frequently employed in laser-cluster experiments. In this method an initial pump-pulse ionizes the cluster. The cluster expands freely before, after a delay time, a probe-pulse hits the expanding cluster. The interaction of this probe pulse with the cluster will sensitively depend on the cluster size and thus on the delay time. We revisit such a scenario in our current work since it will allow us to compare the efficiency of laser energy absorption for such a standard pump-probe method with the single UV pulse scenario which will be introduced in Sec. V.

The laser field profile is of the form $E_{\mathrm{l}}(t) = E_0 \sin^2(\pi t/nT)\cos(\omega_{\mathrm{l}} t)$ for both pump and probe pulse. The time period T is chosen with respect to the wavelength 800 nm. For, say, $n = 4$ the product nT determines the total pulse duration ≈ 11 fs. The pulse envelope and intensity are kept the same for all cases under study, i.e., the laser energy in all pulses is the same too.

Figure 2a shows the results for the Xe_{17256} cluster of initial radius $R_0 \approx 7$ nm at an intensity $5\times10^{16}\mathrm{Wcm}^{-2}$ when both the pump and the probe pulse have the same wavelength 400 nm. The average charge $\mathcal{Z}_{\mathrm{av}}$, the scaled Mie-frequency $\omega_{\mathrm{Mie}}/\omega_{\mathrm{l}}$, the total absorbed energy E_{tot} (electrostatic field energy plus the kinetic energy of electrons and ions), the normalized cluster radius $R(t)/R_0$, and the laser fields are plotted vs time (in units of the period T). During the first four laser cycles of the pump-pulse the average charge state rises to $\mathcal{Z}_{\mathrm{av}} \approx 11$, the frequency $\omega_{\mathrm{Mie}}/\omega_{\mathrm{l}} \approx 2.5$ and $E_{\mathrm{tot}} \approx 2.0\times10^7$ while the cluster expansion is insignificant. The total energy $E_{\mathrm{tot}} \approx 2.0\times10^7$ corresponds to the average energy absorbed per ion $E_{\mathrm{tot}}/N \approx 31.4$ keV. After the pump-pulse the cluster evolves freely and $\mathcal{Z}_{\mathrm{av}}$, E_{tot} remain unchanged but $\omega_{\mathrm{Mie}}/\omega_{\mathrm{l}}$ drops due to the expansion. Note that the cluster radius $R(t)$ (defining the cluster boundary) corresponds to the distance of the most energetic ions from the cluster center. At the boundary, however, the cluster

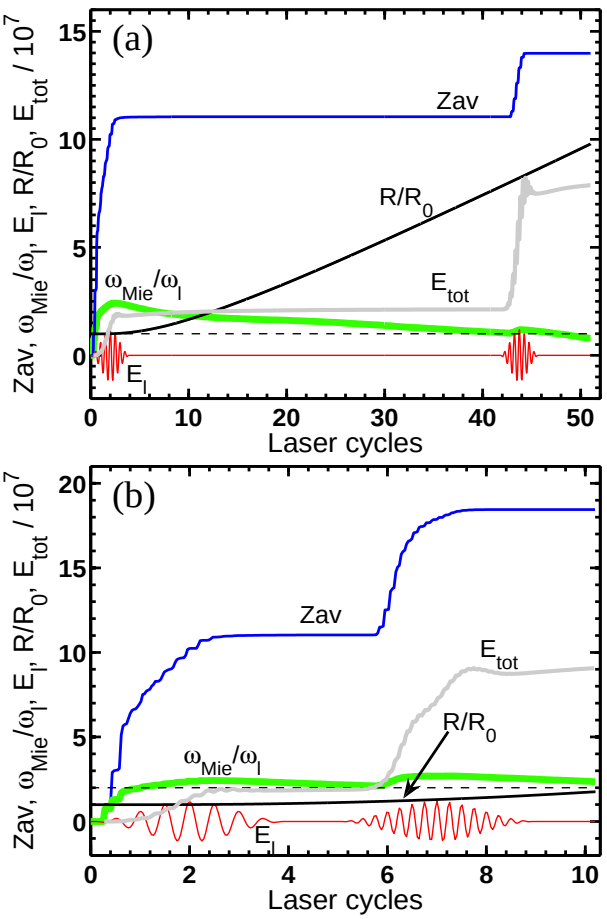

FIG. 2: (Color online) Average ion charge $\mathcal{Z}_{\rm av}$, scaled Mie-frequency $\omega_{\rm Mie}/\omega_{\rm l}$, laser field $E_{\rm l}$ (in atomic units), normalized cluster expansion radius R/R_0 and total absorbed energy $E_{\rm tot}$ (in atomic units) vs time (in 800 nm laser cycles) for a Xe_{17256} cluster of radius $R_0 \approx 7$ nm. The peak intensity $5\times10^{16}{\rm Wcm}^{-2}$ is the same for (a) pump of wavelength 400 nm (probe, 400 nm) and (b) pump of wavelength 400 nm (probe, 200 nm). The laser field is of the form $E_{\rm l}(t) = E_0\sin^2(\pi t/nT)\cos(\omega_{\rm l}t)$ with $n = 4$ and one laser cycle T corresponding to the wavelength 800 nm. A minor increase in $E_{\rm tot}$ after the pulses is an artifact of PIC simulations.

potential is anharmonic. Hence using $R(t)$ for the calculation of the Mie-frequency $\omega_{\rm Mie}(t) = \sqrt{N\mathcal{Z}_{\rm av}/R^3(t)}$ the latter is underestimated. Instead we use the definition $\omega_{\rm Mie}(t) = \sqrt{Q_{\rm b}(t)/R_0^3}$ (as in Ref. [47]) where $Q_{\rm b}(t)$ is the total ionic charge within the *initial* cluster radius R_0 where the cluster potential is close to harmonic at all times.

After 44 laser cycles $\omega_{\rm Mie}$ approaches the linear resonance (dashed line) with respect to the fundamental 400 nm, i.e., $\omega_{\rm Mie}/\omega_{\rm l} = 1$. The probe pulse of wavelength 400 nm is applied with a delay of ≈ 42 laser cycles such that the peak of the pulse approximately coincides with the resonance time. Due to the linear resonance the average charge and the absorbed energy rises abruptly up to the value $\mathcal{Z}_{\rm av} = 14$ and $E_{\rm tot} \approx 7.5\times10^7$, respectively. Such a pump-probe simulation clearly illustrates that the linear resonance indeed plays a role in the cluster dynamics. More energy is absorbed, leading to higher charge states. These results are in agreement with hydrodynamic and Vlasov simulations[11, 26]. However, linear resonance is met only after a relatively long time when the cluster has already expanded significantly (as seen $R(t)/R_0 \approx 8$ in Fig. 2a). Ionization ignition and laser energy absorption in such a low density plasma is expected to be less efficient compared to the case where linear resonance occurs *before* the cluster expands significantly.

While keeping the 400 nm pump as above we now assume a probe wavelength of 200 nm for the purpose of hitting the linear resonance at an earlier time when the cluster is more compact. The energy in the probe pulse is the same as in Fig. 2a. Figure 2b shows the result analogous to Fig. 2a. The average charge and the absorbed energy now increase up to $\mathcal{Z}_{\rm av} = 18.5$ and $E_{\rm tot} \approx 9\times10^7$ which are higher than in Fig. 2a after the probe. With the pulse energies being the same in both cases a higher efficiency of energy absorption in the second scheme (Fig. 2b) is obvious. The reason is the smaller cluster size at the time of linear resonance ($R(t)/R_0 < 1.5$) and the higher space charge field related to it. Similar findings from experiments have been reported in Ref. [11]. In passing we note that the average charge $\mathcal{Z}_{\rm av} \approx 11$ in Fig. 2 due to the pump (at 400 nm) exceeds $\mathcal{Z}_{\rm av} \approx 8$ in Fig. 1b (at 800 nm) for the same cluster and the same laser intensity $5.0\times10^{16}{\rm Wcm}^{-2}$ despite the higher pulse-energy in Fig. 1b because of the twice longer pulse.

In the following section we study the wavelength dependence of the average charge states and the laser energy absorption.

V. IONIZATION AT DIFFERENT WAVELENGTHS

Does the average charge state and the absorbed energy for a given cluster increases with decreasing laser wavelength? One could expect that for a certain wavelength the linear resonance during the initial ionization stage when the Mie-frequency rises from zero to its maximum value becomes important. For long wavelengths this early resonance is passed so quickly due to the rapid charging of the cluster that any indication of a resonance is washed out.

We assume the same laser field profile $E_{\rm l}(t) = E_0\sin^2(\pi t/nT)\cos(\omega_{\rm l}t)$ as in Sec. III with the same pulse duration, pulse energy, and intensity $5.0\times10^{16}{\rm Wcm}^{-2}$ so that the number of laser cycles in the pulse depends on the wavelength. The laser wavelength is varied in the range $800-100$ nm. Note that in the following we specify times and pulse durations in units of laser periods at 800 nm (corresponding to $T \approx 2.6$ fs).

Figure 3 shows the average charge state $\mathcal{Z}_{\rm av}$ and to-

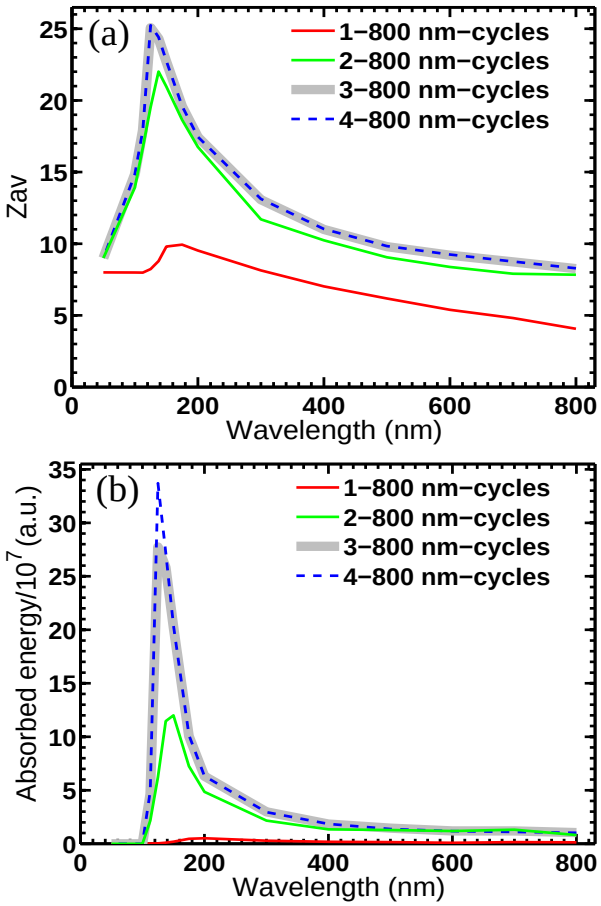

FIG. 3: (Color online) Average ion charge $\mathcal{Z}_{\rm av}$ (a) and total absorbed energy $E_{\rm tot}$ (b) vs laser wavelength after $1, 2, 3$ and 4 laser cycles (at 800 nm) for a Xe_{17256} cluster of radius $R_0 \approx$ 7 nm. Other parameters as in Fig. 2.

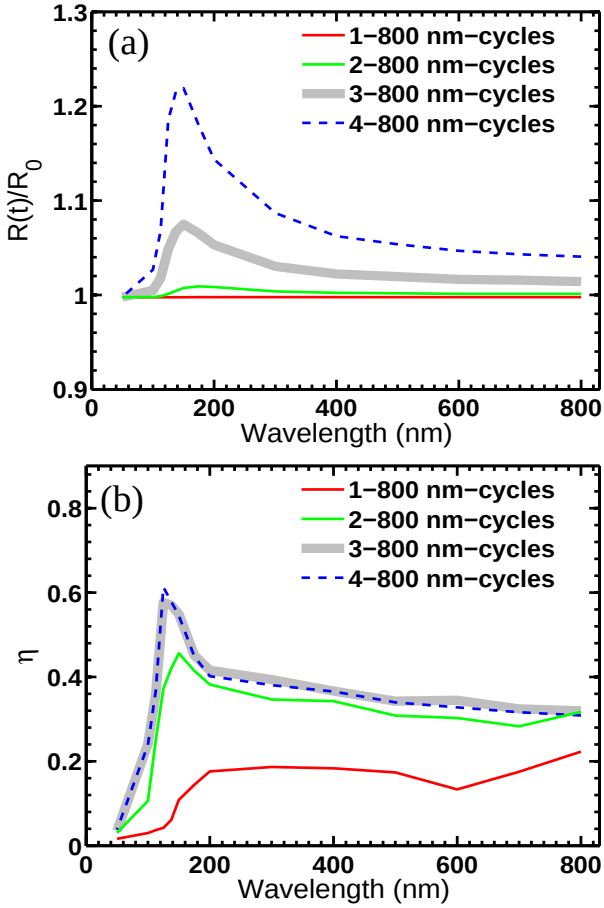

FIG. 4: (Color online) Normalized cluster expansion radius R/R_0 (a) and outer ionization degree η (b) vs laser wavelength, corresponding to Fig. 3.

tal absorbed energy $E_{\rm tot}$ vs the laser wavelength for the Xe_{17256} cluster of radius $R_0 \approx 7$ nm after $t = 1, 2, 3, 4$-laser cycles at 800 nm. The value of $\mathcal{Z}_{\rm av}$ increases in time (in Fig. 3a) for all wavelengths. Ionization mostly occurs before $t = 2$ cycles when the peak of the pulse is reached. After that the space charge field is high enough to generate further charge states between $2 - 3$ cycles. $\mathcal{Z}_{\rm av}$ does not change anymore between $3 - 4$ cycles, indicating a saturation of inner ionization. The average charge state $\mathcal{Z}_{\rm av}$ increases from $\mathcal{Z} = 8$ to a maximum value $\mathcal{Z}_{\rm av} \approx 25$ as the laser wavelength is decreased from the infrared 800 nm down to the UV wavelength 125 nm. It means that the sub-shells $4s^2p^6d^{10}5s^2p^6$ of almost all atoms are empty at 125 nm. A further decrease of the wavelength causes $\mathcal{Z}_{\rm av}$ to decrease gradually to a smaller value $\mathcal{Z}_{\rm av} \approx 9$ at 50 nm.

Figure 3b shows a similar qualitative behavior of the absorbed energy both in the time domain and in the wavelength domain. The energy $E_{\rm tot}$ is maximum at the same wavelength $\lambda_{\rm l} = 125$ nm. Although the laser-pulse energy is the same in all cases the increased absorption at 125 nm, leading to a marked increase of the average charge up to a value $\mathcal{Z}_{\rm av} \approx 25$ clearly shows that wavelength effects are undoubtedly important. One may compare the absorbed energy and the average charge with the dual-pulse simulation results in Fig. 2. The absorbed energy $E_{\rm tot} \approx 34 \times 10^7$ a.u. and the average charge $\mathcal{Z} \approx 25$ are much higher in the present case around the laser wavelength 125 nm compared to the respective values $E_{\rm tot} \approx 9 \times 10^7$ and $\mathcal{Z}_{\rm av} \approx 18.5$ in Fig. 2b. The absorption is ≈ 3.78 times higher than in Fig. 2b. Moreover, in the dual-pulse case the total laser-pulse energy was twice higher. Therefore, the absorption efficiency is augmented further by a factor of two.

In Fig. 4 we plot the normalized expansion radius $R(t)/R_0$ (Fig. 4a) and the outer ionization degree η (number of total electrons outside $R(t)$ divided by the total number of electrons produced, $N\mathcal{Z}_{\rm av}(t)$, in Fig. 4b) vs the laser wavelength corresponding to the results in Fig. 3. The radius $R(t)$ and the outer ionization degree $\eta(t)$ go hand in hand with the absorbed energy $E_{\rm tot}(t)$ and the charge $\mathcal{Z}_{\rm av}(t)$. After four cycles the cluster has expanded very little, $R(4T)/R_0 \approx 1.225$ at

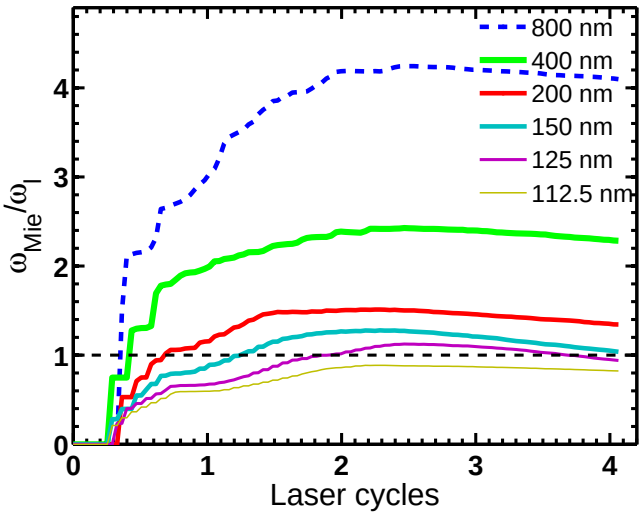

FIG. 5: (Color online) Scaled Mie-frequency $\omega_{\rm Mie}/\omega_{\rm l}$ vs time (in 800 nm cycles) for wavelengths $\lambda_{\rm l} = 800 - 112.5$ nm and the laser and cluster parameters of Fig. 3.

$\lambda_{\rm l} \approx 125$ nm, although the average charge $\mathcal{Z}_{\rm av} \approx 25$ is very high compared to Fig. 2. With such an insignificant expansion the space charge field can be considered optimized, leading to maximum ionization ignition. The ignition field (i.e., the space charge field due to the ionic background) under the assumption that all electrons are removed reads $E_{\rm ig}(t) \approx N\mathcal{Z}_{\rm av}(t)/R(t)^2$. Using $R(t)$ from Fig. 4a and $\mathcal{Z}_{\rm av}(t)$ from Fig. 3a, one obtains at 125 nm $E_{\rm ig}(2T) \approx 20.0$, $E_{\rm ig}(3T) \approx 21.0$ and $E_{\rm ig}(4T) \approx 16.2$, if all electrons are removed (i.e., $\eta = 1$). The expected ignition field ≈ 21 a.u. is maximum near the pulse peak around $2-3$-cycles, thereafter decreases to $E_{\rm ig}(4T) \approx 16.2$ due to an expansion $R(4T)/R_0 \approx 1.225$ and no further creation of charge states. Note that the peak laser field is only $E_0 \approx 1.19$. Therefore the enhanced ionization is certainly due to the ignition field. However, at $\lambda_{\rm l} \approx 125$ nm $\eta \approx 0.6$ in Fig. 4b, meaning that 40% of the electrons are still inside the cluster. The presence of these electrons lowers $E_{\rm ig}$ compared to the above ideal case of $\eta = 100\%$ outer ionization, and one may argue that $E_{\rm ig}$ is not yet optimized. However, even if $\eta = 100\%$ outer ionization is achieved for the above laser field intensity the maximum total field is ≈ 22 which is still insufficient to produce a higher average charge $\mathcal{Z}_{\rm av} = 27$ (requiring a threshold field $\gtrapprox 24$ according to OFI). Hence the average charge state is optimized. This will be shown explicitly at the end of this section where we actually achieve $\eta \approx 100\%$ for this cluster.

The above results clearly show that there exists a certain wavelength at which the laser-cluster coupling is very efficient. Such a nonlinear dependence of the absorbed energy and average charge state on the laser wavelength indicates a resonance around 125 nm in Fig. 3 and 4. To investigate this further, we plot in Fig. 5 the scaled Mie-frequency $\omega_{\rm Mie}(t)/\omega_{\rm l}$ vs time. The dashed line indicates the linear resonance. Charging of the cluster starts around 0.3 cycles for all wavelengths by OFI, leading to an abrupt increase of $\omega_{\rm Mie}(t)/\omega_{\rm l}$ for the longer wavelengths while for the shorter ones the increase proceeds slower. As a result the plasma is overdense during the entire pulse for the long wavelengths but stays close to the linear resonance for the shorter wavelengths. The more time is spent near the linear resonance, the higher is the energy absorption and the average charge state, as seen in Fig. 3. At the wavelength 125 nm the resonance is met at the peak of the pulse so that the energy absorption is particularly efficient.

We now discuss the time evolution of the space charge field $E^x_{\rm sc}$ (along the laser polarization) at different positions inside the cluster to further illustrate the resonance at short wavelengths, leading to efficient ionization ignition and the generation of high charge states. Figure 6 shows the space charge field $E^x_{\rm sc}$ and the laser field $E_{\rm l}$ vs time at radial positions $0.24R_0$, $0.48R_0$, $0.72R_0$ and $0.96R_0$ for four different wavelengths. Figure 7 shows the corresponding phases of $E^x_{\rm sc}$ with respect to the driving laser field.

At the long wavelength 800 nm, $E^x_{\rm sc}$ inside the cluster at radii $0.24R_0$, $0.48R_0$, $0.72R_0$ mostly oscillates with a phase $\delta \approx \pi$ while $\delta \approx 0$ at the boundary (i.e., at $0.96R_0$). This is clearly what one expects from an overdense plasma: screening of the laser field in the cluster interior but an opposite behavior outside the electron cloud. The oscillation of the space charge field arises due to the oscillations of the electrons trapped inside the cluster. These electrons form approximately a sphere which is smaller than the cluster due to outer ionization. If the electron cloud was rigid and did not cross the cluster boundary the phase should be exactly π and 0 inside and outside, respectively, if the plasma is overdense, and opposite in the underdense case. In reality, the bound electron population changes and the electron sphere is neither rigid nor has it a sharp boundary, resulting in phase distortions and deviations from the idealized case, as seen in Fig. 7a.

Figure 6 confirms explicitly that the total field at the boundary is highest and therefore leads to the highest ionic charge states while $E^x_{\rm sc}(t)$ almost nullifies the laser field in the strongly overdense regime. The maximum value of the total field at the peak of the pulse is ≈ 4.0 a.u. (x-component only) which is sufficient to produce charge states up to $\mathcal{Z} \approx 18$ (also seen in Fig. 1b). An additional contribution (up to a factor $\sqrt{3}$) to the total field comes from the y and z-components of the space charge field.

At 200 nm the amplitude of $E^x_{\rm sc}$ around $t = 1.5$ cycles at $0.24R_0$ increases up to 5 a.u. which, after addition to the laser field, is sufficient to produce charge states $\mathcal{Z} = 18$ even inside the cluster. After ≈ 1.75 cycles $E^x_{\rm sc}$ at $0.72R_0$ behaves similarly to that at $0.96R_0$, i.e., the laser and space charge fields at $0.96R_0$ and $0.72R_0$ are now approximately in phase. Figure 6b shows that the total field $\approx 4-8$ between $0.96R_0$ and $0.72R_0$, producing charge states $\mathcal{Z} \approx 18 - 23$. However, due to the screen-

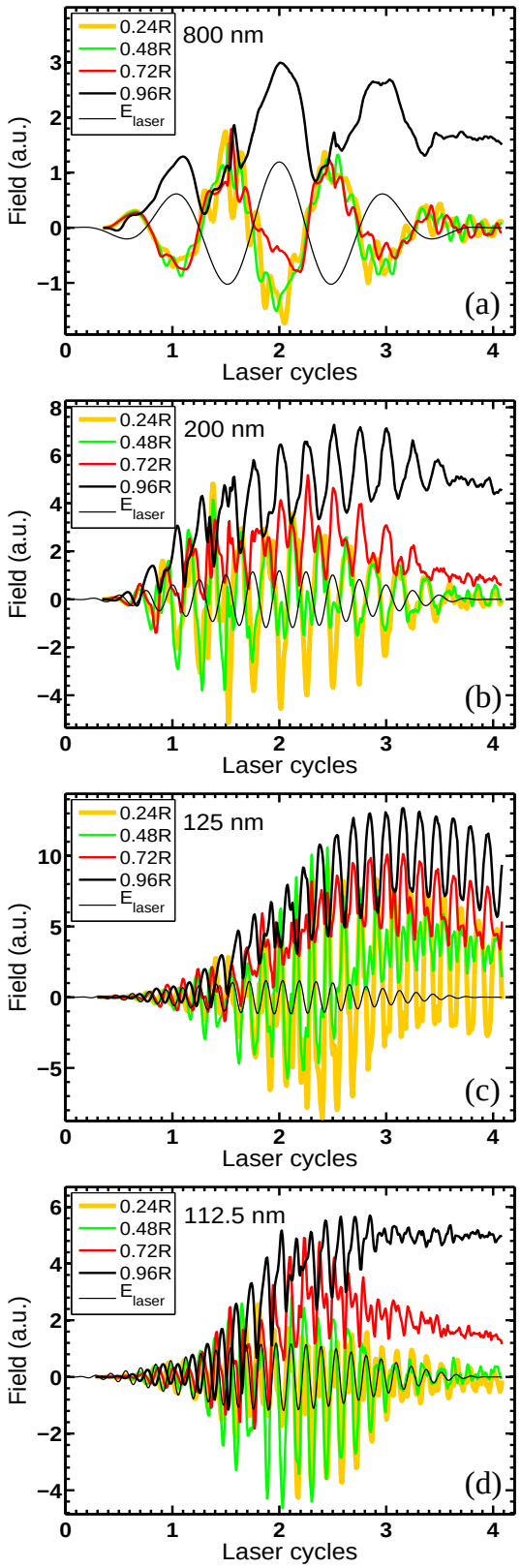

FIG. 6: (Color online) The x-component of the space charge field at radial distances $0.24R_0, 0.48R_0, 0.72R_0$, and $0.96R_0$ inside a Xe_{17256} cluster of radius $R_0 \approx 7$ nm and the laser field $E_l(t) = E_0 \sin^2(\pi t/nT)\cos(\omega_l t)$ of peak intensity $5 \times 10^{16}\mathrm{Wcm}^{-2}$ vs time (in periods corresponding to 800 nm) at (a) $\lambda_l = 800$, (b) $\lambda_l = 200$, (c) $\lambda_l = 125$, and (d) $\lambda_l = 112.5$ nm.

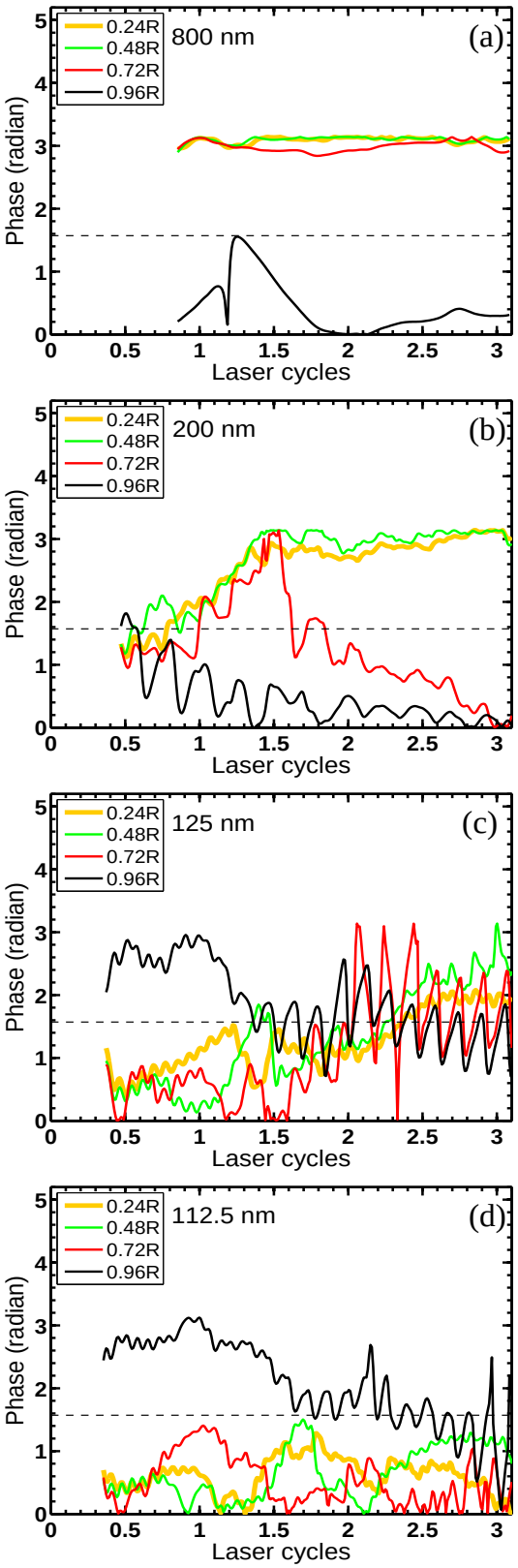

FIG. 7: (Color online) Phase of the space charge field with respect to the laser field at different radial distances corresponding to Fig. 6 vs time corresponding to Fig. 6.

ing of the laser field inside the cluster, many atoms there have only charge states $\mathcal{Z} < 18$ so that the average charge state is $\mathcal{Z}_{\rm av} \approx 18$ in Fig. 3. From Fig. 7b it is seen that before $t = 1.75$ cycles the phase of $E^x_{\rm sc}$ at $0.72R_0$ approximately follows the phase at the smaller radii $0.24R_0$ and $0.48R_0$ since the plasma is evolving from under to overdense. Then, with increasing outer ionization and thus shrinking electron sphere, $E^x_{\rm sc}$ at $0.72R_0$ drops and approaches the behavior for $0.96R_0$.

At the resonant wavelength 125 nm violent oscillations of the electron cloud are driven, leading to a particularly high total field everywhere inside the cluster and an average charge state $\mathcal{Z}_{\rm av} \approx 25$ in Fig. 3. Higher charge states $\mathcal{Z} > 26$ are not produced because of the high threshold field ≈ 24 necessary to crack the M-shell. One may argue that the presence of 40% electrons inside the cluster (in Fig. 4b) will deplete the field inside significantly. However, one should keep in mind that at resonance the electron cloud oscillates with a large excursion, exposing a substantial part of the naked ionic background, leading to an enhanced "dynamical ionization ignition" [18] which can produce higher charge states than expected from the laser field alone even inside the cluster. Finally, after $t = 3$ cycles $E^x_{\rm sc}$ at the boundary drops due to the cluster expansion. As expected, the phases plotted in Fig. 7c fluctuate around $\pi/2$ throughout the cluster once the resonance condition is met.

At 112.5 nm the plasma remains underdense. Figure 6d shows that the space charge field amplitudes drop compared to those in Fig. 6c, yielding less ionization ignition and absorbed energy, similar to the 200 nm-case.

Even in the optimal 125 nm case presented so far only 60% of the generated electrons were removed from the cluster (visible in Fig. 4b). Therefore outer ionization and ionization ignition was certainly not optimized. We argued that even if the remaining 40% electrons were removed, the average charge state would not be significantly increased as compared to that shown in Fig. 3a. To prove that, we performed PIC simulations for the same cluster and the same peak intensity but now employing two consecutive pulses (shown in Fig. 8). The first pulse of resonant wavelength 125 nm with respect to the still compact cluster is ramped up over four 800 nm-cycles and held constant afterwards up to 8 cycles (the details of how the pulse is ramped down do not matter; therefore it is simply switched off abruptly). At $t = 8$ cycles a second pulse is switched on (over 2 cycles) whose frequency is resonant with the Mie-frequency around $t = 10$ cycles.

After the first pulse the cluster doubled its radius, and the outer ionization degree amounts to $\eta(R) \approx 0.8$ so that 20% electrons are still inside the cluster of radius $R(t)$ while $\approx 10\%$ are inside a sphere of radius R_0. The average charge $\mathcal{Z}_{\rm av}$ in Fig. 8b does not change significantly compared to Fig. 3a although the pulse energy per unit area $\int_0^{8T} E_{\rm l}^2(t)\,{\rm d}t$ is $\approx 3-4$ times higher.

The purpose of the second pulse shown in Fig. 8b is the removal of the residual electrons. Although almost 95% outer ionization within the expanding radius R and

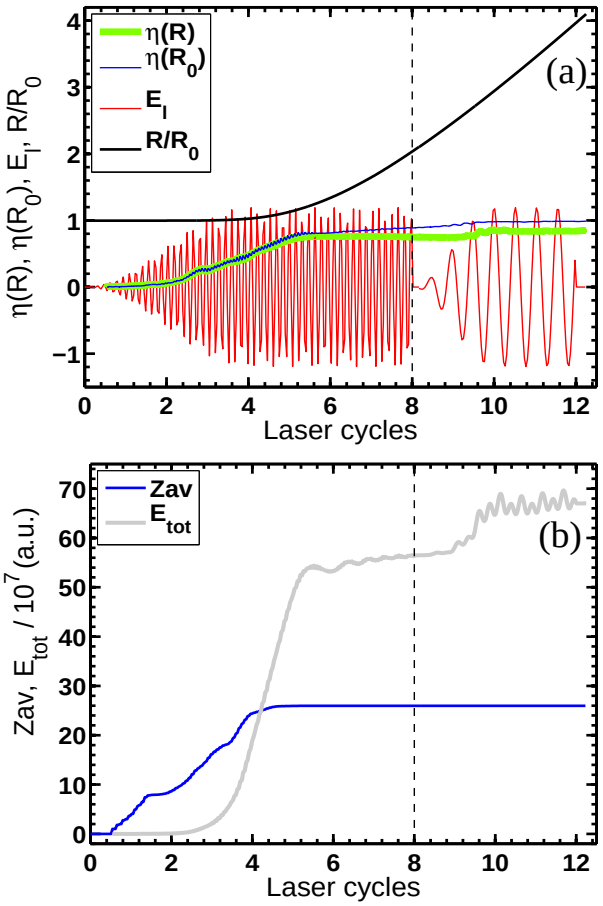

FIG. 8: (Color online) Variation of (a) normalized cluster radius R/R_0, degree of outer ionization $\eta(R), \eta(R_0)$ within R and R_0, laser field $E_{\rm l}$ (in atomic units) (b) average ion charge $\mathcal{Z}_{\rm av}$ and total absorbed energy $E_{\rm tot}$ in time (in units of the laser period T corresponding to 800 nm) for the Xe_{17256} cluster of Fig. 3. The two laser pulses of wavelength 125 and 415 nm, respectively, are included in (a). The peak intensity is the same as in Fig. 3 for both pulses.

99% within R_0 are achieved, no higher charge states are created. The absorbed energy also does not rise significantly so that the higher input energy invested into the two pulses does not pay off. Hence a single, short UV-pulse of wavelength 125 nm turns out to be optimal with respect to fractional energy absorption and generation of a high average charge state under the conditions considered.

VI. SUMMARY

In summary, we studied the interaction of xenon clusters with intense short laser pulses using a three-dimensional PIC code. Our aim was to optimize for a given cluster the laser energy absorption and the generation of high average charge states. The latter will then lead to energetic ions upon Coulomb explosion. We

showed that for a given laser intensity an optimal laser wavelength exists that, under the typical conditions studied in this work, lies in the UV regime. Energy absorption is optimized when resonance is met during an early stage of the dynamics when the cluster is still compact. The conventional, long-pulse linear resonance during the expansion of the cluster is less efficient.

Acknowledgments

We thank Sergei Popruzhenko for valuable discussions and careful proofreading. This work was supported by the Deutsche Forschungsgemeinschaft.

[1] T. Ditmire, J.W.G. Tisch, E. Springate, M.B. Mason, N. Hay, J. Marangos, and M.H.R. Hutchinson, Nature (London) **386**, 54 (1997).
[2] T. Ditmire, R.A. Smith, J.W.G. Tisch, and M.H.R. Hutchinson, Phys. Rev. Lett. **78**, 3121 (1997).
[3] T. Ditmire, Contemporary Physics, **38**, 315 (1997).
[4] T. Ditmire, J.W.G. Tisch, E. Springate, M.B. Mason, N. Hay, J.P. Marangos, and M.H.R. Hutchinson, Phys. Rev. Lett. **78**, 2332 (1997).
[5] V. Kumarappan, M. Krishnamurthy, and D. Mathur, Phys. Rev. Lett. **87**, 85005 (2001).
[6] V. Kumarappan, M. Krishnamurthy, D. Mathur, and L.C. Tribedi Phys. Rev. A **63**, 023203 (2001).
[7] M. Krishnamurthy, D. Mathur, and V. Kumarappan, Phys. Rev. A **69**, 033202 (2004).
[8] M. Krishnamurthy, J. Jha, D. Mathur, Ch. Jungreuthmayer, L. Ramunno, J. Zanghellini and T. Brabec, J. Phys. B: At. Mol. Opt. Phys., **39**, 625 (2006).
[9] M. Lezius, S. Dobosz, D. Normand, and M. Schmidt Phys. Rev. Lett. **80**, 261 (1998).
[10] V. Kumarappan, M. Krishnamurthy, and D. Mathur, Phys. Rev. A **66**, 033203 (2002).
[11] E. Springate, N. Hay, J.W.G. Tisch, M.B. Mason, T. Ditmire, M.H.R. Hutchinson, and J.P. Marangos, Phys. Rev. A **61**, 063201 (2000).
[12] E. Springate, S.A. Aseyev, S. Zamith, and M.J.J. Vrakking, Phys. Rev. A **68**, 053201 (2003).
[13] Y. L. Shao, T. Ditmire, J. W. G. Tisch, E. Springate, J. P. Marangos, and M. H. R. Hutchinson, Phys. Rev. Lett. **77**, 3343 (1996).
[14] V. Kumarappan, M. Krishnamurthy, and D. Mathur, Phys. Rev. A **67**, 043204 (2003).
[15] L.M. Chen, J.J. Park, K.H. Hong, I.W. Choi, J.L. Kim, J. Zhang and C.H. Nam, Phys. Plasmas **9**, 3595 (2002).
[16] U. Saalmann and J.M. Rost, J. Phys. B: At. Mol. Opt. Phys. **39**, R39-R77 (2006).
[17] C. Rose-Petruck, K.J. Schafer, K.R. Wilson, and C.P.J. Barty, Phys. Rev. A **55**, 1182 (1997).
[18] D. Bauer and A. Macchi, Phys. Rev. A **68**, 033201 (2003).
[19] K. Ishikawa and T. Blenski, Phys. Rev. A **62**, 063204 (2000).
[20] F. Megi, M. Belkacem, M.A. Bouchene, E. Suraud, and G. Zwicknagel, J. Phys. B: At. Mol. Opt. Phys. **36**, 273 (2003).
[21] C. Jungreuthmayer, M. Geissler, J. Zanghellini, and T. Brabec, Phys. Rev. Lett. **92**, 133401 (2004).
[22] D. Bauer, J. Phys. B: At. Mol. Opt. Phys. **37**, 3085 (2004).
[23] I. Last and J. Jortner, Phys. Rev. Lett. **87**, 033401 (2001), I. Last and J. Jortner, J. Phys. Chem. A **106**, 10877 (2002), I. Last and J. Jortner, J. Chem. Phys. **121**, 8329 (2004).
[24] M. Hohenberger, D.R. Symes, K.W. Madison, A. Sumeruk, G. Dyer, A. Edens, W. Grigsby, G. Hays, M. Teichmann, and T. Ditmire, Phys. Rev. Lett. **95**, 195003 (2005)
[25] J. Jha, D. Mathur, and M. Krishnamurthy, Appl. Phys. Lett. **88**, 041107 (2006).
[26] T. Döppner, Th. Fennel, Th. Diederich, J. Tiggesbäumker, and K.H. Meiwes-Broer, Phys. Rev. Lett. **94**, 013401 (2005).
[27] Yuji Fukuda, Koichi Yamakawa, Yutaka Akahane, Makoto Aoyama, Norihiro Inoue, Hideki Ueda, and Yasuaki Kishimoto, Phys. Rev. A **67**, 061201 (2003).
[28] T. Döppner, Th. Fennel, P. Radcliffe, J. Tiggesbäumker, and K.-H. Meiwes-Broer, Phys. Rev. A **73**, 031202(R) (2006).
[29] Th. Fennel, T. Döppner, J. Passig, Ch. Schaal, J. Tiggesbäumker, and K.-H. Meiwes-Broer, Phys. Rev. Lett. **98**, 143401 (2007).
[30] C. Siedschlag and J.M. Rost, Phys. Rev. A **71**, 031401 (2005).
[31] T. Martchenko, Ch. Siedschlag, S. Zamith, H. G. Muller, and M. J. J. Vrakking, Phys. Rev. A **72**, 053202 (2005).
[32] K. Kondo, A. B. Borisov, C. Jordan, A. McPherson, W. A. Schroeder, K. Boyer, and C. K. Rhodes, J. Phys. B **30**, 2707 (1997).
[33] W. A. Schroeder, F. G. Omenetto, A. B. Borisov, J. W. Longworth, A. McPherson, C. Jordan, K. Boyer, K. Kondo, and C. K. Rhodes, J. Phys. B **31**, 5031 (1998).
[34] A. McPherson, B. D. Thompson, A. B. Borisov, K. Boyer, and C. K. Rhodes, Nature (London) **370**, 631 (1994).
[35] H. Wabnitz *et al.*, Nature (London) **420**, 482 (2002).
[36] S. Namba, N. Hasegawa, M. Nishikino, T. Kawachi, M. Kishimoto, K. Sukegawa, M. Tanaka, Y. Ochi, K. Takiyama, and K. Nagashima, Phys. Rev. Lett. **99**, 043004 (2007).
[37] G.M. Petrov and J. Davis, Phys. Plasmas **13**, 033106 (2006).
[38] T. Ditmire, T. Donnelly, A.M. Rubenchik, R.W. Falcone, and M.D. Perry, Phys. Rev. A **53**, 3379 (1996).
[39] J. Davis, G.M. Petrov, and A. Velikovich, Phys. Plasmas **14**, 060701 (2007).
[40] G.M. Petrov, J. Davis, A.L. Velikovich, P.C. Kepple, A. Dasgupta, R.W. Clark, A.B. Borisov, K. Boyer, and C.K. Rhodes, Phys. Rev. E **71**, 036411 (2005).
[41] L. Köller, M. Schumacher, J. Köhn, S. Teuber, J. Tiggesbäumker, and K.H. Meiwes-Broer, Phys. Rev. Lett. **82**, 3783 (1999).
[42] S. Zamith, T. Martchenko, Y. Ni, S.A. Aseyev, H.G. Muller, and M.J.J. Vrakking, Phys. Rev. A **70**, 011201(R) (2004).
[43] I. Last and J. Jortner, Phys. Rev. A **60**, 2215 (1999).
[44] Ulf Saalmann and Jan-Michael Rost, Phys. Rev. Lett.

91, 223401 (2003).
[45] Th. Fennel, G.F. Bertsch, and K.H. Meiwes-Broer, Eur. Phys. J. D **29**, 367 (2004).
[46] M. Kundu and D. Bauer, Phys. Rev. A **74**, 063202 (2006).
[47] M. Kundu, S.V. Popruzhenko, and D. Bauer, Phys. Rev. A **76**, 033201 (2007).
[48] H.A. Bethe and E.E. Salpeter, *Quantum mechanics of one- and two-electron atoms* (Plenum Publishing Corporation, New York, 1977).
[49] J. Andruszkow *et al.*, Phys. Rev. Lett. **85**, 3825 (2000).
[50] V. Ayvazyan *et al.*, Phys. Rev. Lett. **88**, 104802 (2002).
[51] C. Siedschlag and J.M. Rost, Phys. Rev. Lett. **93**, 043402 (2004).
[52] C. Jungreuthmayer, L. Ramunno, J. Zanghellini and T. Brabec, J. Phys. B: At. Mol. Opt. Phys. **38**, 3029, (2005).
[53] M. Kundu and D. Bauer, Phys. Rev. Lett. **96**, 123401 (2006).
[54] P. Mulser and M. Kanapathipillai, Phys. Rev. A **71**, 063201 (2005); P. Mulser, M. Kanapathipillai, and D.H.H. Hoffmann, Phys. Rev. Lett. **95**, 103401 (2005).
[55] T. Taguchi, T.M. Antonsen, Jr., and H.M. Milchberg, Phys. Rev. Lett. **92**, 205003 (2004); Thomas M. Antonsen, Jr. Toshihiro Taguchi, Ayush Gupta, John Palastro, and Howard M. Milchberg, Phys. Plasmas **12**, 056703 (2005).